Belhocine et al. 2014. *Int. J. Vehicle Structures & Systems*, 6(3), 64-70
ISSN: 0975-3060 (Print), 0975-3540 (Online)
doi: 10.4273/ijvss.6.3.04


**International Journal of Vehicle Structures & Systems**
Available online at www.maftree.org/eja

# Dry Contact and Coupled Thermomechanical Analyses of Brake Disc-Pad using Finite Element Simulation

**Ali Belhocine[a], Nouby Mahdi Ghazali[b] and Oday Ibraheem Abdullah[c]**

[a]*Faculty of Mechanical Engg.,*
*Oran University of Science & Technology, Algeria.*
*Corresponding Author, Email: al.belhocine@yahoo.fr*

[b]*Mechanical Engg. Dept.,*
*Faculty of Engg., South Valley University, Egypt.*
*Email: nouby.ghazaly@eng.svu.edu.eg*

[c]*System Technology and Mechanical Design Methodology,*
*Hamburg University of Technology, Germany.*
*Email: oday.abdullah@tu-harburg.de*

**ABSTRACT:**

*The motivation of this work is to identify the thermal effects on the structural and contact behaviour of a disc-pad assembly using a finite element approach. The first analysis is performed on the disc-pad model without the presence of thermal properties. Structural performance of the disc-pad model such as deformation and Von Mises stress is predicted. Next, thermomechanical analysis is performed on the same disc-pad model with the inclusion of convection, adiabatic and heat flux elements. The prediction results of temperature distribution, deformation, stress and contact pressure are presented. Comparison of the structural performance between the mechanical and thermomechanical is also made. Three disc-pad designs are assessed using the developed finite element model.*

**KEYWORDS:**

*Finite element analysis; Braking system; Disc-pad interface; Temperature; Deformation; Stress; Contact pressure*

**CITATION:**

A. Belhocine, N.M. Ghazali and O.I. Abdullah. 2014. Dry Contact and Coupled Thermomechanical Analyses of Brake Disc-Pad using Finite Element Simulation, *Int. J. Vehicle Structures & Systems*, 6(3), 64-70. doi:10.4273/ijvss.6.3.04.

## 1. Introduction

In basic working operation, a disc brake system has to reduce wheel speed when a driver desires vehicle deceleration. The kinetic energy generated by a vehicle in terms of wheel speed is converted into heat energy due to the application of the brake. The friction force between disc and brake pad applies friction torque to the wheel in the opposite direction of the car's movement. This results in a reduction of vehicle speed and heat energy occurring in the brake disc causes a temperature increment in the disc swept area during the brake application. This physical action of the brake disc causes heat conduction to the adjacent braking system components [1]. Lee [2] stated that inconsistent dissipation of heat inside the brake disc could cause deformation of the disc. The disc deformation could also cause friction loss and consequently led to brake fade [3]. High temperature of the brake disc could cause cracking in the brake disc material due to high thermal stresses and vibrations [4, 5].

It is become common in the brake research community to fully utilize finite element (FE) approach in order to identify and predict disc brake structural performance. For instance, Koetniyom [6] performed temperature analysis on brake discs under heavy operating conditions. He found that the physical shape of vehicle brake discs play a significant role in determining the temperature characteristics including the overall brake efficiency. Kamnerdtong et al. [7] attempted to link the interaction between mechanical and thermal effects with disc movements and heat caused by friction. They concluded from FE analysis that the temperature on the disc surface changed at each point over the period, which indicates inconsistent dissipation and temperature differences in each side of the disc. Inconsistent contact between disc and pad could affect material deformation.

Akhtar et al. [8] employed FE method to explain the transient thermoelastic phenomena of a dry clutch system. The effect of sliding speed on contact pressure distribution, temperature and heat flux generated along the frictional surfaces was analyzed. Sowjanya and Suresh [9] conducted a static structural analysis of the disc brake with selected composite materials to compare the results obtained such as deflection and stresses. In the research by Reddy et al.[10], thermal and structural coupled analysis was carried out to find the strength of the disc brake. Gnanesh et al. [11] investigated thermal-structural analysis of solid and vented disc brake using FE approach in the case of design with and with out holes in the disc. The materials used in the simulation were cast iron, stainless steel and aluminum metal matrix composites. Manjunath and Suresh [12] performed a

structural and thermal analysis of the disc brake using FE method to determine the deformation and the Von Mises stress established in the disc for the both solid and ventilated discs with two different materials to enhance performance of the disc. In the work carried out by Parab et al. [13], structural and thermal analysis was carried out on the disc brakes using stainless steel, cast iron and carbon-carbon composite. Structural analysis was done on the disc brake to assess the strength of the disc brake, whilst thermal analysis was performed to analyze the thermal effect on the disc brake behavior. Tiwari et al.[14] carried out a transient structural analysis of disc brake to determine the variation of the stresses and deformation across the disc brake profile.

The aim of this paper was to investigate the structural and contact behaviours of the brake disc and pads during the braking phase with and without thermal effects. Firstly, total deformation of the disc-pads model at the time of braking, stress and contact distributions of the brake pads were determined. Later, results of the thermoelastic coupling such as Von Mises stress, contact pressure field and total deformations of the disc and pads were also presented which will be useful in the brake design process for the automobile industry.

## 2. FE modelling & constraints

In this work, a three-dimensional FE model consisting a ventilated disc and two pads is employed as illustrated in Fig. 1. Fig. 2 shows contact zone between the disc and pad. Details of the mesh properties are given in Table 1. The selected material for the disc is grey cast iron FG 15 with high carbon content and the brake pad has an isotropic elastic behaviour. The mechanical properties are given in Table 2. Design parameters of the brake components are given in Table 3. The structural deformation, stress, temperature and contact pressure distributions of the disc brake during braking are simulated using ANSYS version 11.

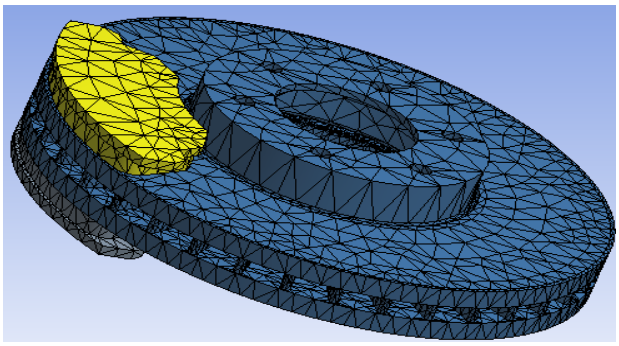

**Fig. 1: FE model of disc-pad assembly**

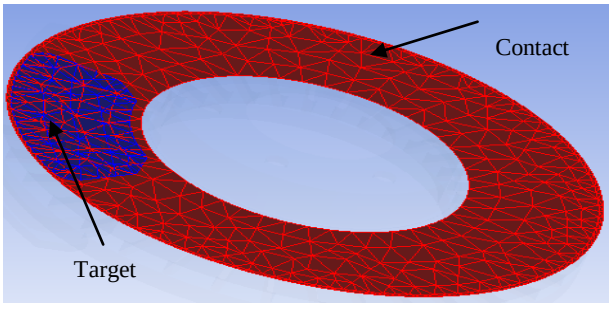


**Fig. 2: Triangular quadratic contact zones of disc and pad**

**Table 1: FE model properties**

| Description | Nodes | Elements |
|---|---|---|
| Disc | 34799 | 18268 |
| Pad 1 | 1446 | 650 |
| Pad 2 | 1461 | 660 |
| Contact zone 1 | 0 | 914 |
| Contact zone 2 | 0 | 83 |

**Table 2: Thermoelastic properties of disc and pad**

| Property | Disc | Pad |
|---|---|---|
| Elastic modulus $E$ (GPa) | 138 | 1 |
| Poisson's ratio υ | 0.28 | 0.25 |
| Density ρ(kg/m$^3$) | 7250 | 1400 |
| Coefficient of friction μ | 0.2 | 0.2 |
| Thermal conductivity, K (W/m°C) | 57 | 5 |
| Specific heat, c (J/Kg°C) | 460 | 1000 |

**Table 3: Design parameters of disc and pad**

| Design parameter | Disc | Pad |
|---|---|---|
| Volume (m$^3$) | 9.5e-4 | 8.5e-5 |
| Surface (m$^2$) | 0.2 | 1.8e-2 |
| Mass (kg) | 6.9 | 0.4 |
| Inertia moment Ip1 (kg·m²) | 3.5e-2 | 2.7e-5 |
| Inertia moment Ip2 (kg·m²) | 6.9e-2 | 1.5e-4 |
| Inertia moment Ip3 (kg·m²) | 3.5e-2 | 1.2e-4 |

The value of contact pressure between the disc and pad is presumed constant. It is supposed that 60% of the braking forces are supported by the front brakes (both discs), that is to say 30% for a single disc [15]. The force of the disc for a typical vehicle is calculated using the vehicle data contained in Table 4, resulting in working forces to the brake disc,

$$F_{disc} = \frac{(30\%)\frac{1}{2} m v_0^2}{\frac{2R_{rotor}}{R_{tire}}\left(v_0 t_{stop} - \frac{1}{2}\left\{\frac{v_0}{t_{stop}}\right\} t_{stop}^2\right)} = 1047.36\ N \qquad (1)$$

The rotational speed of the disc is calculated using,

$$\omega = \frac{v_0}{R_{tire}} = 157.89\ rad/s \qquad (2)$$

Total disc surface area in contact with pads is 35797 mm$^2$. The hydraulic pressure [16] is obtained using,

$$P = \frac{F_{disc}}{A_c \mu} = 1\ MPa \qquad (3)$$

Where $A_c$ is the surface area of the pad in contact with the disc and $\mu$ is the friction coefficient.

**Table 4: Vehicle data**

| Parameter | Value |
|---|---|
| Vehicle mass $m$ (kg) | 1385 |
| Initial velocity $v_0$ (m/s) | 60 |
| Duration of braking $t_{stop}$ (s) - | 45 |
| Effective radius of the disc (mm) | 100.5 |
| Radius of the wheel (mm) | 380 |
| Pad surface area $A_d$ (mm$^2$) | 5246.3 |

The imposed boundary conditions on the FE model are shown in Fig. 3(a) and 3(b) for applied pressure on one and two side(s) of the pad respectively. The disc is

rigidly constrained in all directions except in its rotational direction at the bolt holes. The pad is fixed at the abutment in all degrees of freedom except in the normal direction to allow the pads move up and down and in contact with the disc surface [17]. To express the heat transfer in the disc brake model, thermal boundary conditions and initial condition have to be defined. As shown in Fig. 4, at the interface between the disc and brake pads, heat is generated due to sliding friction. In the exposed region of the disc and brake pads, it is assumed that heat is exchanged with the environment through convection [18]. On the surface of the back plate, adiabatic surface boundary condition is used.

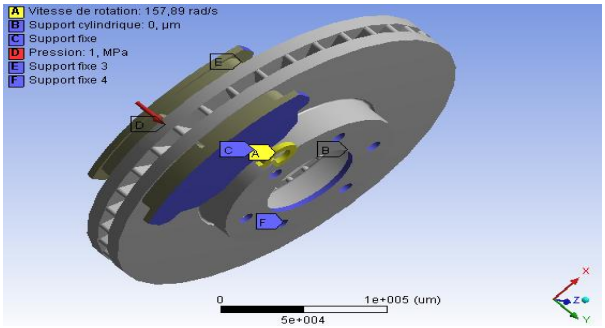


**Fig. 3(a): Boundary conditions and applied pressure on one side of the disc-pads**

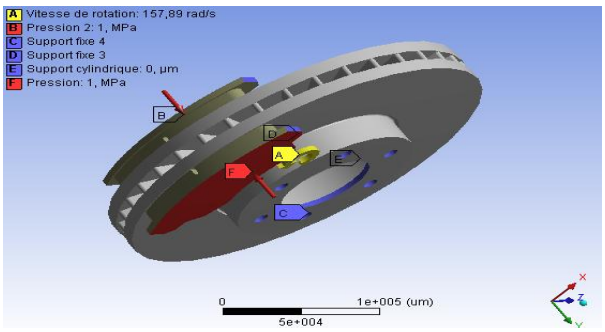


**Fig. 3(b): Boundary conditions and applied pressure on two sides of the disc-pads**

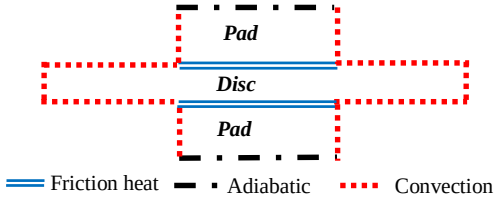


**Fig. 4: Thermal boundary conditions for analysis of the disc brake**

## 3. Contact algorithm

Surface-to-surface contact is most efficient for bodies that experience large values of relative sliding such as a block sliding on a plane or sphere sliding within groove [19]. In this analysis, surface-to-surface contact is used due to larger areas of clutch elements in contact. To model the frictional contact, 8-noded CONTA174 element is utilized. This contact is employed in the 3-D structural and coupled field contact analyses. The contact element permits the use of both isotropic and orthotropic friction models. In this case, an isotropic friction model was used with a variable coefficient ranging between 0.35 and 0.55 and a starting value of 0.45 that correspond to the coupling materials. An uniform stick-slip behavior in all directions is considered. For the CONTA174 element, the rate of frictional dissipation is evaluated using the frictional heating factor as,

$$q = FHTG\ \tau V \tag{4}$$

Where $\tau$ is the equivalent frictional stress. $V$ is the sliding rate and FHTG is the fraction of frictional dissipated energy converted into heat (a default value of 1 was used). The amount of frictional dissipation on contact and target surfaces is given by,

$$q_c = F_W F_f t v \tag{5}$$

$$q_T = (1 - F_W) F_f t v \tag{6}$$

Where $q_c$ is the amount of frictional dissipation on the contact side. $q_T$ is the amount of frictional dissipation on the target side and $F_W$ is a weighted distribution factor (a default value of 0.5 was used). The relationships presented previously are valid only for the sliding mode of friction and a coefficient of friction greater than zero. To take into account of the conductive heat transfer between contact and target surface, a real constant thermal contact conductance coefficient, TCC, is specified using,

$$q = TCC \cdot (T_t - T_c) \tag{7}$$

Where $q$ is the heat flux per area. $T_t$ and $T_c$ is the temperature at the contact points on the target and contact surfaces.

In this work, a penalty method in ANSYS has been chosen. This penalty method uses a contact "spring stiffness" to establish a relationship between the two contact surfaces as shown in Fig. 5. The contact force between two bodies can be written as,

$$F_n = k_n x_p \tag{8}$$

Where $k_n$ is the contact stiffness and $x_p$ is the distance between two existing nodes (penetration or gap). The stiffness relationship between contact and target surfaces will decide the amount of the penetration. Higher values of contact stiffness will decrease the amount of penetration but can lead to ill conditioning of the global stiffness matrix and convergence difficulties. Lower values of contact stiffness can lead to a certain amount of penetration that is low enough to facilitate the convergence of the solution.The contact stiffness for an element of area $A$ is calculated using [20]:

$$F_{kn} = \int \{f_i\}(e)\{f_i\}^T dA \tag{9}$$

The default value of the contact stiffness factor is 1 which is appropriate for bulk deformation. If bending deformation dominates the solution, contact stiffness factor of 0.1 is recommended.

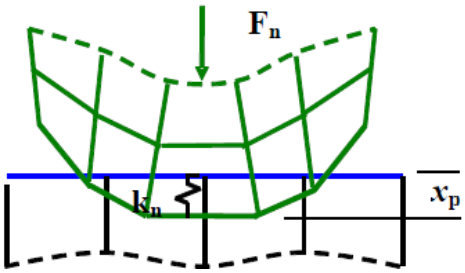


**Fig. 5: Contact stiffness between the disc and pad**

## 4. Dry contact mechanical model results and discussions

The mechanical model without thermal effects is analysed using ANSYS. Fig. 6 shows the disc and pad deformation over the simulated braking duration. The deformation plots at selective time steps are shown in Fig. 8. It is noted that the large deformation is always found at the outer radius of the disc that is the area in contact with the pad. The predicted peak deformation is 53 µm at t = 3.5s and afterward. The peak deformation for pads is located at the outer radial region as depicted in Fig. 9. The pads are less deformed compared to the disc. At braking time of t= 3.5s and afterward, the maximum deformation of the pads is predicted as 19 µm which is 64% lower than that of the disc.

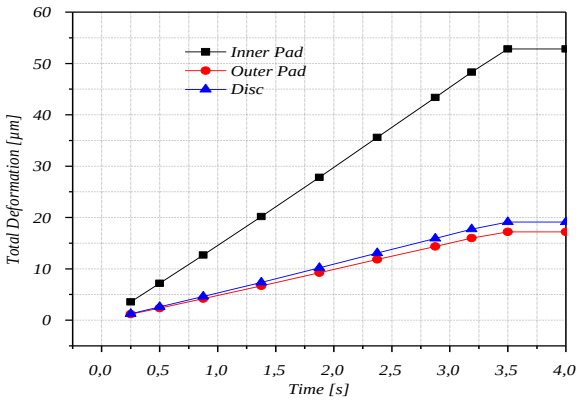


**Fig. 6: Deformation of disc and pads vs. Braking time**

Fig. 7 shows the stress distribution at braking time t = 45s across the inner pad contact surface. The equivalent Von Mises stress is distributed almost symmetrically between the leading and trailing sides of the pad as shown in Fig. 10. These stress distributions are barely unchanged over braking time except the stress value. It shows that the stress increases gradually and it reaches its maximum value of 5.3 MPa at braking time of 3.5s and afterward. The peak stress is predicted on the left side and the outer radius of the pad. It can be seen that more uniform stress distribution occurs at lower radius of the pad compared to the outer radius and center region of the pad. In addition, the highest stress is generated on the right and left side at the outer radius and the center region of the pad respectively.

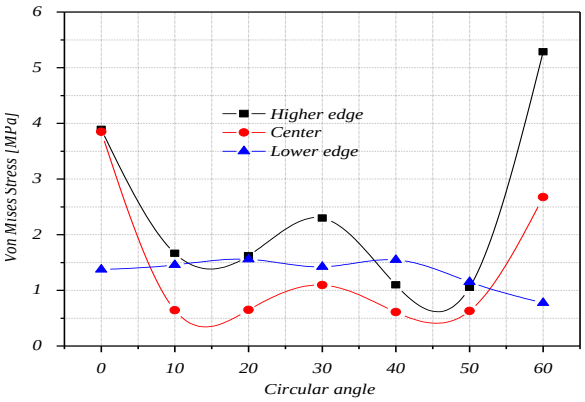


**Fig. 7: Von Mises stress at different angular positions of the pad**

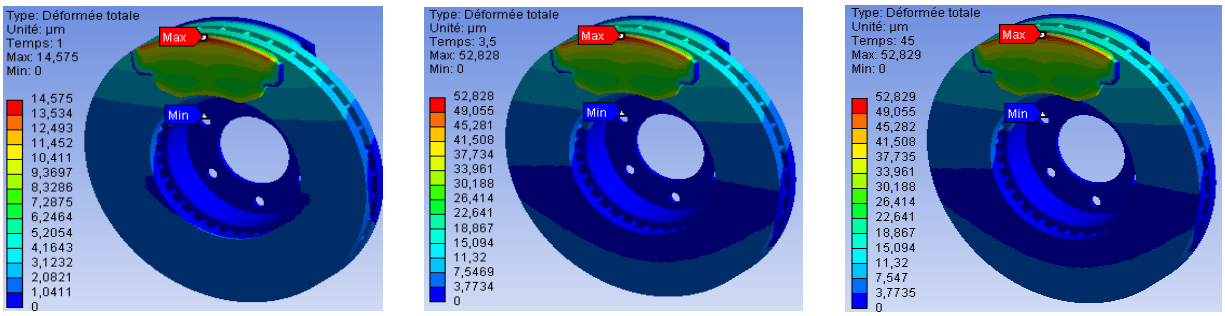


At time t = 1s | At time t = 3.5s | At time t =45s

**Fig. 8: Disc deformation (µm) at different braking time**

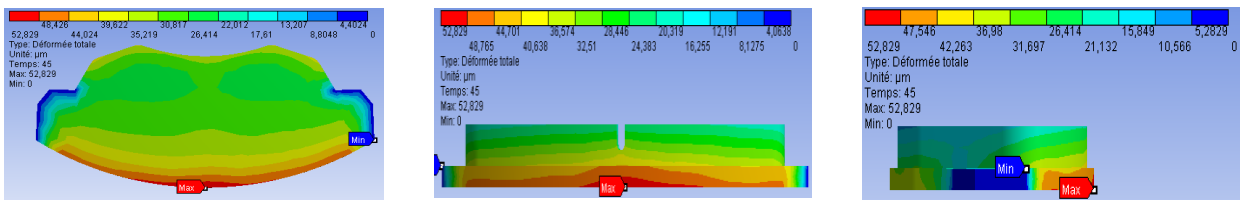


Front view | View from below | Right view

**Fig. 9: Pad deformation (µm) at braking time t = 45s**

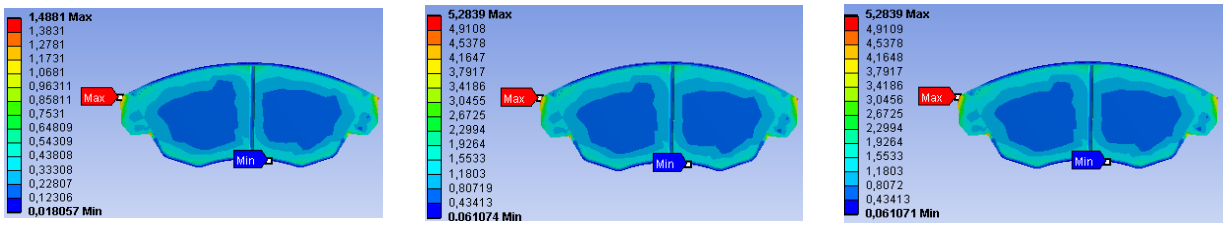


At time t = 1s | At time t = 3.5s | At time t =45s

**Fig. 10: Von Mises stress (MPa) distribution of the pad at different braking time**

## 5. Thermomechanical model results and discussions

In this section, structural and thermal analyses are coupled using ANSYS Multiphysics to identify the stress levels and global deformations of the model studied during the braking phase under the effect of temperature. The initial temperature of the disc and pads is set at 20 °C. Surface convection condition is applied to all surfaces of the disc and the convection coefficient of 5 W/m$^2$°C is applied at the surface of the two pads. At braking time of 1.7s the disc and pad surface generates quite high temperature, i.e. 346 °C as shown in Fig. 11. However, the upper part of the backplate shows a lower temperature approximately at 90°C. This is caused by the effect of convection of ambient air.

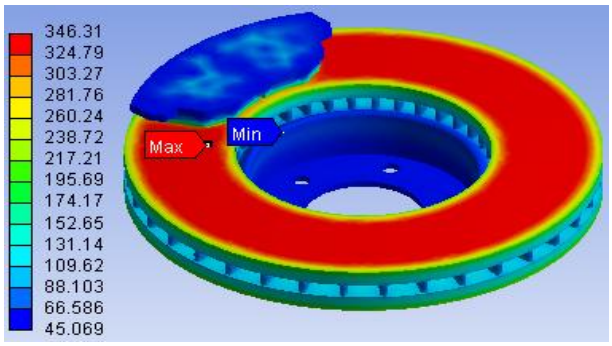


**Fig. 11: Temperature ($^o$ C) distribution of the disc and pads at braking time t = 1.7s**

Fig. 12 shows the deformations at the nodes located in the mean and outer radius of the disc. The deformation at the outer radius of the disc is higher than the deformation at the mean radius. The curves indicate umbrella phenomenon which is resulting from the heating of non-parallel paths of friction with respect to their initial position. It is also observed that the disc deformation increases linearly as a function of the disc radius as shown in Fig. 13. The peak deformation is predicted at an angular position of 90$^o$. From Fig. 14, it is shown that the disc deforms severely under the effect of temperature. For instance at the braking time of 3.5s, the disc with thermal effects deforms at 280 µm as compared to 53 µm for the disc without thermal effects. The maximum displacement is localized on the slopes of friction, the fins and the outer ring as shown in Fig. 15.

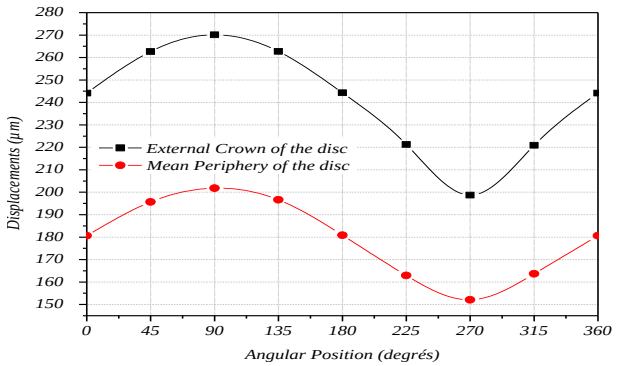


**Fig. 12: Disc deformation (µm) at the mean and outer radius over angular positions at braking time t = 3.5s**

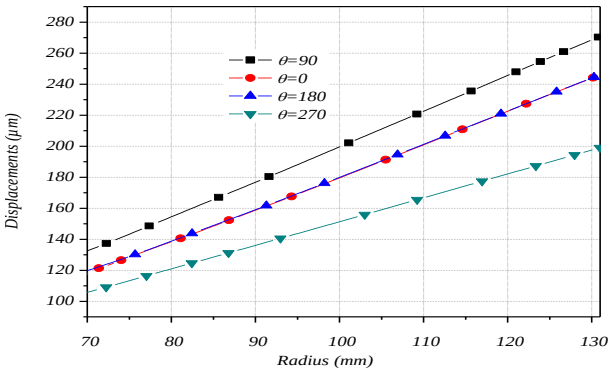


**Fig. 13: Disc deformation (µm) at different radius and angular positions at braking time t = 3.5s**

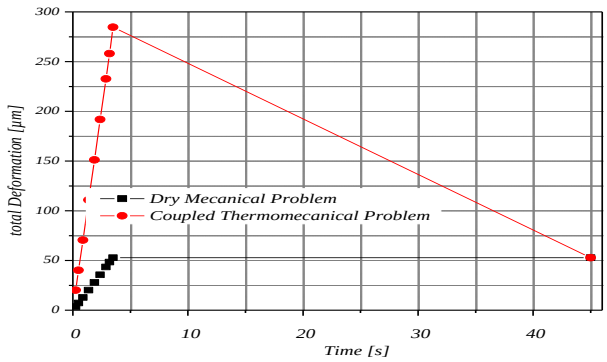


**Fig. 14: Disc deformation (µm) with and without thermal effects**

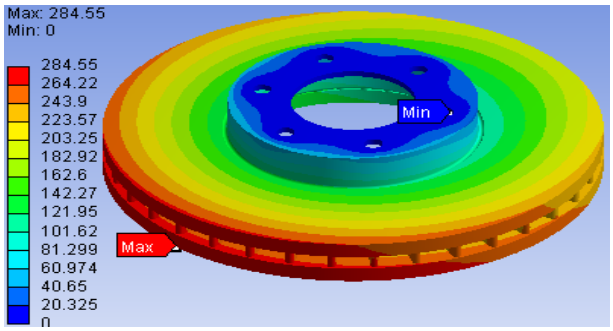


**Fig. 15: Total deformation (µm) of the disc with thermomechanical coupling**

The influence of the pad groove and single & dual piston loading on the equivalent Von Mises stress distribution is studied. The stress distribution for three pad designs are shown in Fig. 16(a)-16(d). It shows that at the beginning of braking time (t = 1.7s) most of the pads experienced low stress as expected. At braking time t = 45s, the stress level has been increased. The presence of the groove and double piston loading provide a positive effect on the stress distribution for the pad.

The contact pressure distribution along the lower, middle and upper radius of the disc-pad interface at braking time t = 1.7s with pad surface temperature T = 346°C is shown in Fig. 17. The contact pressure curves are almost identical in shape for three different regions of the pad. At 30$^o$ angle, contact pressure is predicted higher at the lower pad radius followed by the outer pad radius and middle pad radius. When the thermal and mechanical aspects are coupled, the contact pressure distribution of the pads increases in a notable way as seen in Fig. 18.

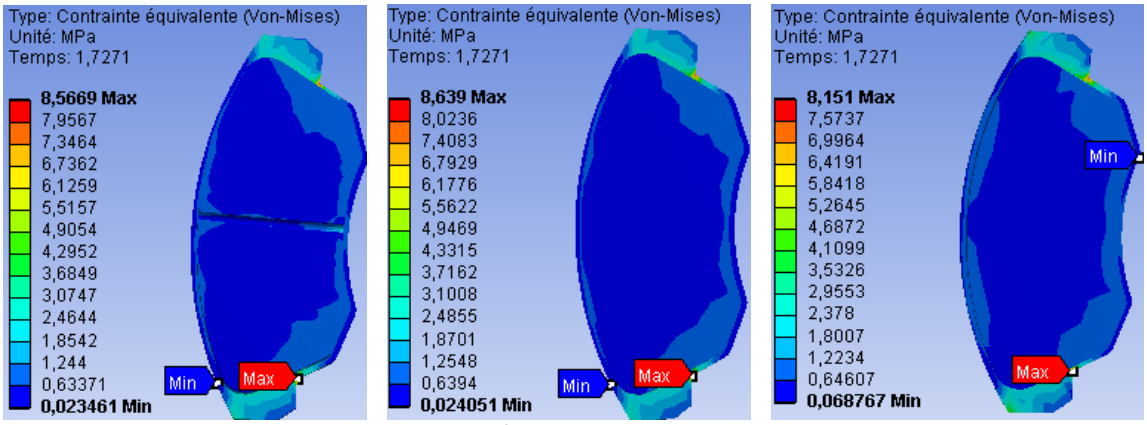


At time t = 1.7s

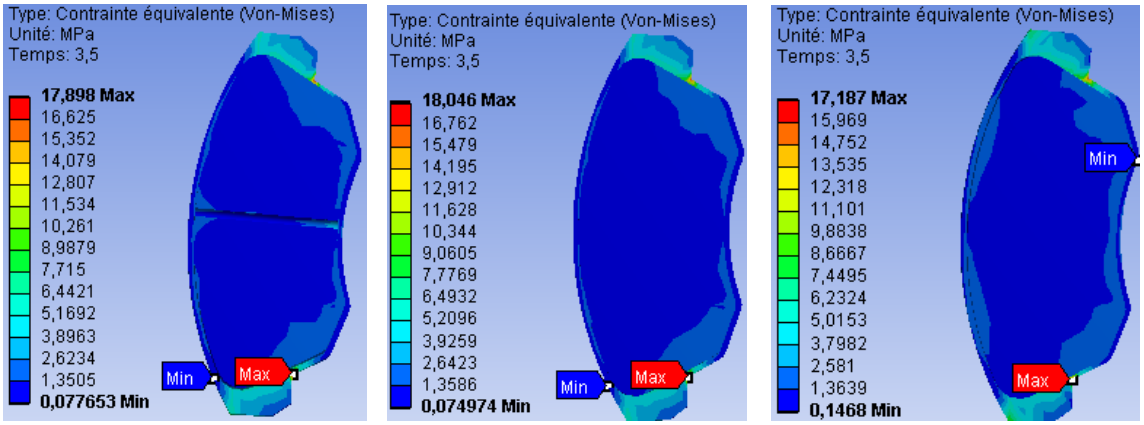


At t time t = 3.5s

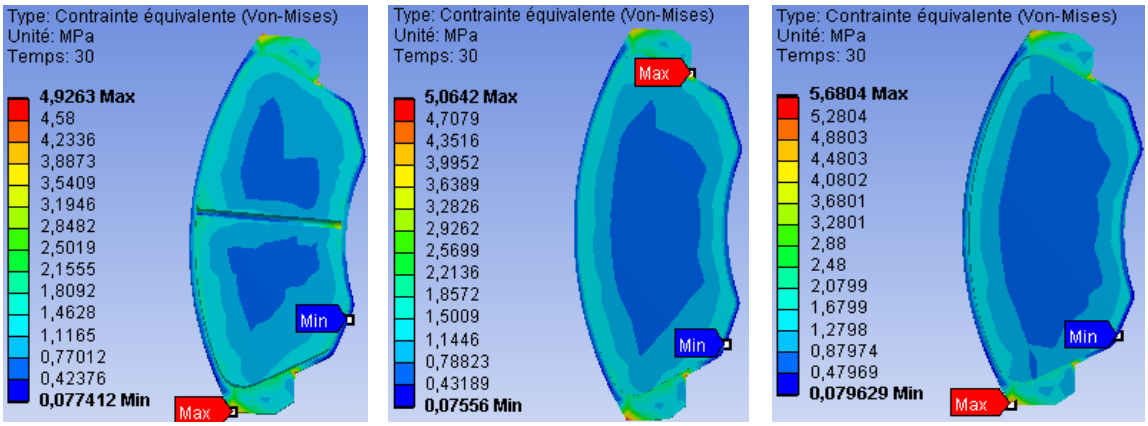


At time t = 30s

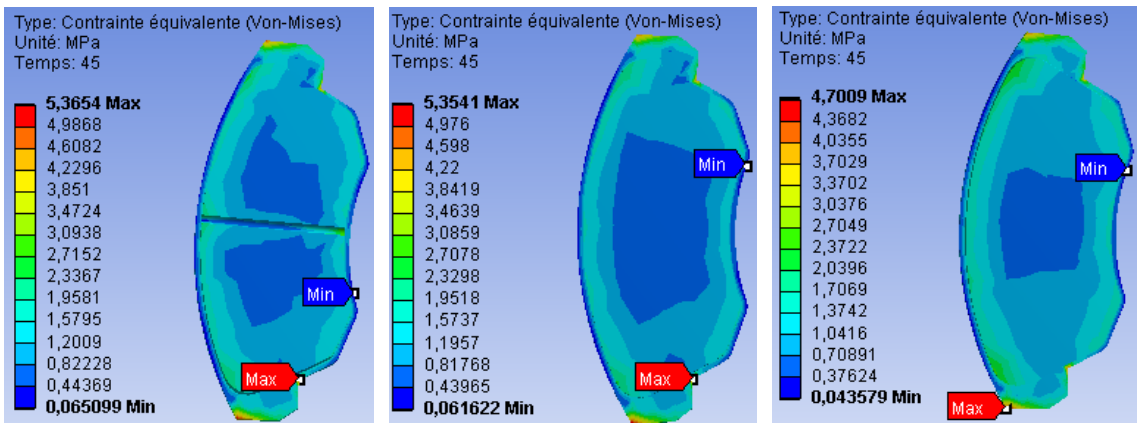


At time t = 45s

**Fig. 18: Distribution of Von Mises stress at different braking time: Single piston with center groove (left), Single piston without groove (center) and Double piston without groove (right)**

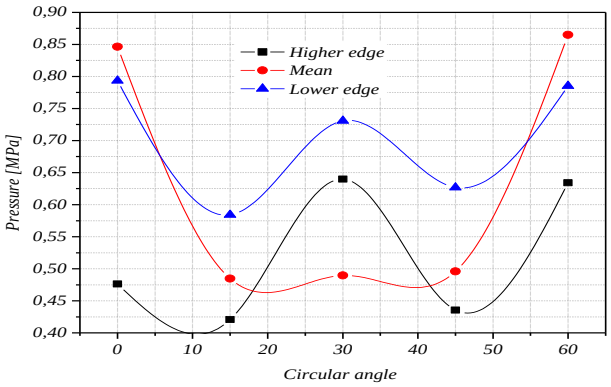


**Fig. 19: Distribution of contact pressure along the lower, middle and upper radius of the pad at time t=1.7s**

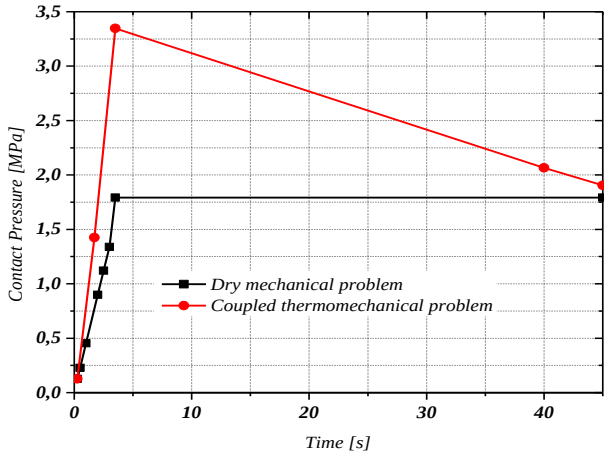


**Fig. 20: Contact pressure of the inner pad**

## 6. Conclusions

In this work, a disc brake-pad model has been assessed using mechanical and thermomechanical analyses. Three pad designs are simulated to identify their influence on the stress distribution. Large deformation is occurred at the outer radius of the disc. More uniform stress distribution is noticed for the pad without groove and with a double-piston loading. Temperature has a significant effect on the structural and contact behaviour of the disc brake assembly. Large deformation and high contact pressure is found in the disc-pad model when the thermal effects are included.

## REFERENCES:

[1] S. Lakkam, K. Suwantaroj, P. Puangcharoenchai, P. Mongkonlerdmanee and S. Koetniyom. 2013. Study of heat transfer on front-and back-vented brake discs, *Songklanakarin J. Sci. Tech.*, 35(6), 671-681.

[2] K. Lee. 1999. Numerical prediction of brake fluid temperature rise during braking and heat soaking, *SAE Technical Paper* 1999-01-0483.

[3] G. Cueva, A. Sinatora, W.L. Guesser and A.P. Tschiptschin. 2003. Wear resistance of cast irons used in brake disc rotors, *Wear*, 255, 1256-1260. http://dx.doi.org/10.1016/S0043-1648(03)00146-7.

[4] F. Bergman, M. Eriksson and S. Jacobson. 1999. Influence of disc topography on generation of brake squeal, *Wear*, 225-229, 621-628. http://dx.doi.org/10.1016/S0043-1648(99)00064-2.

[5] A. Papinniemia, C.S. Laia Joseph, J. Zhaob and L. Loader. 2002. Brake squeal: A literature review, *Applied Acoustics*, 63, 391-400. http://dx.doi.org/10.1016/S0003-682X(01)00043-3.

[6] S. Koetniyom. 2003. Temperature analysis of automotive brake discs, *J. King Mongkut's University of Technology North Bangkok*, 13, 36-42.

[7] T. Kamnerdtong, S. Chutima and A. Siriwattanpolkul. 2005. Analysis of temperature distribution on brake disc, *Proc. 19th Int. Conf. Mech. Engg. Network of Thailand*, Phuket, Thailand.

[8] M.M.J. Akhtar, I.O. Abdullah and J. Schlattmann. 2013. Transient thermoelastic analysis of dry clutch system, *Machine Design*, 5(4), 141-150.

[9] K. Sowjanya and S. Suresh. 2013. Structural analysis of disc brake rotor, *Int. J. Computer Trends and Tech.*, 4(7), 2295-2298.

[10] V.C. Reddy, M.G. Reddy and G.H. Gowd. 2013. Modeling and analysis of FSAE car disc brake using FEM, *Int. J. Emerging Technology and Advanced Engg.*, 3(9), 383-389.

[11] P. Gnanesh, C. Naresh and S.A. Hussain. 2014. Finite element analysis of normal and vented disc brake rotor, *Int. J. Mech. Eng. & Rob. Res.*, 3(1), 27-33.

[12] T.V. Manjunath and P.M. Suresh. 2013. Structural and thermal analysis of rotor disc of disc brake, *Int. J. Innovative Research in Science*, 2(12), 7741-7749.

[13] V. Parab, K. Naik and A.D. Dhale. 2014. Structural and thermal analysis of brake disc, *Int. J. Engg. Development and Research*, 2(2), 1398-1403.

[14] A.K. Tiwari, P. Yadav, H.S. Yadav and S.B. Lal. 2014. Finite element analysis of disc brake by ANSYS Workbench, *Int. J. Research in Engg. & Advanced Tech.*, 2(2), 1-6.

[15] T.J. Mackin, S.C. Noe, K.J. Ball, B.C. Bedell, D.P. Bim-Merle, M.C. Bingaman, D.M. Bomleny, G.J. Chemlir, D.B. Clayton and H.A. Evans. 2002 .Thermal cracking in disc brakes, *Engg. Failure Analysis*, 9, 63-76. http://dx.doi.org/10.1016/S1350-6307(00)00037-6.

[16] G. Oder, M. Reibenschuh, T. Lerher, M. Šraml, B. Šamec and I. Potrč. 2009. Thermal and stress analysis of brake discs in railway vehicles, *Int. J. Advanced Engg.*, 3(1), 95-102.

[17] N. Coudeyras. 2009. *Non-linear Analysis of Multiple Instabilities to the Rubbing Interfaces, Application to the Squealing of Brake*, PhD Thesis, Central School of Lyon, France.

[18] A.R. Abu Bakar, H. Ouyang, L.C. Khai, and M.S. Abdullah. 2010. Thermal analysis of a disc brake model considering a real brake pad surface and wear, *Int. J. Vehicle Structures & Systems*, 2(1), 20-27. http://dx.doi.org/10.4273/ijvss.2.1.04.

[19] O.I. Abdullah and J. Schlattmann. 2013. Contact analysis of a dry friction clutch system, *ISRN Mechanical Engg.*, 1-9. http://dx.doi.org/10.1155/2013/495918.

[20] G.A. Mohr. 1980. Contact stiffness matrix for finite element problems involving external elastic restraint, *Computers & Structures*, 12(2), 189-191. http://dx.doi.org/10.1016/0045-7949(80)90005-X.